

The 2008 October *Swift* detection of X-ray bursts/outburst from the transient SGR-like AXP 1E 1547.0–5408

G. L. Israel,^{1*} P. Esposito,^{2,3} N. Rea,^{4,5} S. Dall’Osso,¹ F. Senziani,^{2,6}
P. Romano,⁷ V. Mangano,⁷ D. Götz,⁸ S. Zane,⁹ A. Tiengo,² D. M. Palmer,¹⁰
H. Krimm,^{11,12} N. Gehrels,¹¹ S. Mereghetti,² L. Stella,¹ R. Turolla,^{13,9}
S. Campana,¹⁴ R. Perna,¹⁵ L. Angelini¹¹ and A. De Luca,^{2,6}

¹INAF/Osservatorio Astronomico di Roma, via Frascati 33, 00040 Monteporzio Catone, Italy

²INAF/Istituto di Astrofisica Spaziale e Fisica Cosmica - Milano, via E. Bassini 15, 20133 Milano, Italy

³INFN - Istituto Nazionale di Fisica Nucleare, Sezione di Pavia, via A. Bassi 6, 27100 Pavia, Italy

⁴Institut de Ciències de l’Espai (ICE-CSIC, IEEC), Campus UAB, Facultat de Ciències, Torre C5-parell, 2a planta, 08193, Barcelona, Spain

⁵University of Amsterdam, Astronomical Institute Anton Pannekoek, Kruislaan 403, 1098 SJ Amsterdam, The Netherlands

⁶IUSS - Istituto Universitario di Studi Superiori, viale Lungo Ticino Sforza 56, 27100 Pavia, Italy

⁷INAF/Istituto di Astrofisica Spaziale e Fisica Cosmica - Palermo, via Ugo La Malfa 153, 90146 Palermo, Italy

⁸CEA Saclay, DSM/Irfu/Service d’Astrophysique, Orme des Merisiers, Bât. 709, 91191 Gif sur Yvette, France

⁹University College London, Mullard Space Science Laboratory, Holmbury St. Mary, Dorking, Surrey RH5 6NT, UK

¹⁰Los Alamos National Laboratory, Los Alamos, New Mexico 87545, USA

¹¹NASA Goddard Space Flight Center, Greenbelt, Maryland 20771, USA

¹²Universities Space Research Association, 10211 Wincopin Circle, Suite 500, Columbia, MD 21044

¹³Università degli Studi di Padova, Dipartimento di Fisica, via F. Marzolo 8, 35131 Padova, Italy

¹⁴INAF/Osservatorio Astronomico di Brera, Via Bianchi 46, 23807 Merate (Lc), Italy

¹⁵JILA, University of Colorado, Boulder, CO 80309-0440, USA

Accepted 2010 May 11. Received 2010 April 9; in original form 2009 October 21

ABSTRACT

We report on the detailed study of the 2008 October outburst from the anomalous X-ray pulsar (AXP) 1E 1547.0–5408 discovered through the *Swift*/Burst Alert Telescope (BAT) detection of SGR-like short X-ray bursts on 2008 October 3. The *Swift*/X-ray Telescope (XRT) started observing the source after less than 100 s since the BAT trigger, when the flux ($\sim 6 \times 10^{-11}$ erg cm⁻² s⁻¹ in the 2–10 keV range) was >50 times higher than its quiescent level. *Swift* monitored the outbursting activity of 1E 1547.0–5408 on a daily basis for approximately three weeks. This strategy allowed us to find a phase-coherent solution for the source pulsations after the burst, which, besides P and \dot{P} , requires a positive \ddot{P} term (spin-down increase). The time evolution of the pulse shape is complex and variable, with the pulsed fraction increasing from 20% to 50% within the *Swift* observational window. The XRT spectra can be fitted well by means of a single component, either a power-law (PL) or a blackbody (BB). During the very initial phases of the outburst the spectrum is hard, with a PL photon index $\Gamma \sim 2$ (or $kT \sim 1.4$ keV) which steepens to $\Gamma \sim 4$ (or $kT \sim 0.8$ keV) within one day from the BAT trigger, though the two components are likely present simultaneously during the first day spectra. An *INTEGRAL* observation carried out five days after the trigger provided an upper limit of $\sim 2 \times 10^{-11}$ erg cm⁻² s⁻¹ to the emission of 1E 1547.0–5408 in the 18–60 keV band.

Key words: stars: neutron – X-rays: bursts – X-rays: individual: 1E 1547.0–5408.

1 INTRODUCTION

Magnetars are a small class of isolated X-ray pulsars, believed to have the highest magnetic fields known to date ($\sim 10^{14}$ –

10^{15} G; Duncan & Thompson 1992; Thompson & Duncan 1993). This class comprises the Anomalous X-ray Pulsars (AXPs) and the Soft Gamma-ray Repeaters (SGRs), observationally very similar in many respects (see Mereghetti 2008 for a recent review): a spin period in the 2–12 s range, large period derivatives (10^{-13} – 10^{-10} s⁻²), unpredictable bursting activity on different timescales (from

* E-mail: gianluca@mporzio.astro.it

ms to hundreds of seconds) and luminosities (10^{38} – 10^{46} erg s⁻¹). Until not long ago AXPs were thought as persistent and stable X-ray sources. Only in 2003 the first transient AXP was discovered by *RXTE*, namely XTE J1810–197, which displayed a factor of >100 flux enhancement with respect to the pre-outburst luminosity level as seen by the *ROSAT* and *Einstein* missions ($\sim 10^{33}$ erg s⁻¹; Ibrahim et al. 2004; Israel et al. 2004; Gotthelf et al. 2004; Gotthelf & Halpern 2005; Bernardini et al. 2009).

Even more surprising was the discovery of a highly variable pulsed radio emission which followed the XTE J1810–197 outburst (Camilo et al. 2006; Helfand et al. 2007), never observed before in any other magnetar (Burgay et al. 2006). Moreover, the transient nature of this AXP provided the first hint that a relatively large number of members of this class has not been discovered yet, and suggested that others would manifest themselves in the future through a phenomenology (outburst) similar to that displayed by XTE J1810–197.

Indeed, after this first discovery, two more transient AXPs have been detected showing similar outbursts, CXOU J164710.2–455216, (Muno et al. 2007; Israel et al. 2007a) and 1E 1547.0–5408. The latter AXP was first suggested as a candidate magnetar in the supernova remnant G327.24–0.13 through X-ray observations (Gelfand & Gaensler 2007), and subsequently recognized as a radio transient magnetar through the discovery of radio pulsations (Camilo et al. 2007b, 2008) at a period of ~ 2.1 s, and of an X-ray outburst (Halpern et al. 2008). In particular, *Swift*/X-ray Telescope (XRT) observations taken in Summer 2007 revealed 1E 1547.0–5408 at an X-ray flux level of $\sim 5 \times 10^{-12}$ erg cm⁻² s⁻¹ (more than one order of magnitude brighter than in quiescence), with characteristics similar to those of XTE J1810–197 in outburst. No X-ray bursts were observed during the 2007 outburst of 1E 1547.0–5408, possibly due to a sparse X-ray coverage. More generally, the first phases of the 2003 and 2007 X-ray outbursts from XTE J1810–197 and 1E 1547.0–5408, respectively, were missed.

Relatively deep *XMM-Newton* pointings were obtained in August 2006 and 2007, the first during quiescence, and the second during the outburst decay. Pulsed fractions of about $\sim 15\%$ and $\sim 7\%$ were inferred for the 2006 and 2007 observations, respectively (Halpern et al. 2008). The 2006 quiescent spectrum ($\sim 4 \times 10^{-13}$ erg cm⁻² s⁻¹ in the 1–10 keV range) can be fitted well with the usual thermal (blackbody) plus non-thermal (power-law) model ($kT = 0.40$ keV and $\Gamma = 3.2$; Halpern et al. 2008), with a 1D resonant cyclotron scattering model (with a surface temperature $kT=0.33$ keV, an electron velocity $\beta=0.32$ and an optical depth $\tau=1.0$; Rea et al. 2008), or with 3D Monte Carlo model (with a surface temperature of $kT=0.33$ keV, an electron bulk velocity of $\beta_{bulk}=0.15$, and a twist angle of $\Delta\phi=1.14$; Zane et al. 2009). On the other hand, the 2007 spectrum ($\sim 3 \times 10^{-12}$ erg cm⁻² s⁻¹ in the 1–10 keV range) is characterized by a harder emission with $kT = 0.52$ keV and $\Gamma = 1.8$ (by using the BB plus PL model).

Deep infrared observations taken from ESO–VLT during the 2007 outburst have revealed four objects consistent with the radio AXP position, although none of them showed variability (Mignani et al. 2009). Recently, during the giant outburst detected from 1E 1547.0–5408 on 2009 January 22, a relatively bright transient IR source ($K_s \sim 18.5$ mag) was discovered within the radio positional uncertainty region of the source (Israel et al. 2009).

Within the magnetar scenario, AXP outbursts are thought to be caused by large scale rearrangements of the external magnetic field, either accompanied or triggered by fracturing of the neutron-star crust. These events may result in renewed magnetospheric activity through the interaction between thermal surface photons and

charges flowing along the (closed) field lines. In addition, hot spots on the neutron-star surface may appear where the currents impact on the star. Repeated resonant cyclotron scatterings onto the magnetospheric particles result in a modification of the seed thermal spectrum with the appearance of a non-thermal, high-energy tail (Thompson et al. 2002).

During the first month since the onset of an outburst, the source experience a large flux variations (approximately by one or two orders of magnitudes). In this respect, monitoring campaigns, obtained just after the outburst onset, are giving an important opportunity to track the evolution of the main physical parameters and, therefore, to check the goodness of the (empirical and/or more physical) components used to model the spectra. Here we report on the discovery of bursting activity and a new outburst from 1E 1547.0–5408, as observed by *Swift* (§2), which was promptly triggered by the onset of the bursting activity of this transient AXP on 2008 October 3. The *Swift* monitoring of the source in the 100 s–22 days time interval allowed us to carry out a detailed timing and spectral study, the first ever for this source, of the initial phases of its outburst on a daily basis. We also report on the results of an *INTEGRAL* Target of Opportunity observation performed during the X-ray outburst (§3), and discuss our findings in comparison with other magnetar outbursts (§4).

2 SWIFT OBSERVATIONS AND DATA ANALYSIS

The *Swift* satellite (Gehrels et al. 2004) is an efficient observatory for the discovery and the multiwavelength monitoring of AXP bursting activity. Whenever the wide-field coded-aperture mask Burst Alert Telescope (BAT; Barthelmy et al. 2005) triggers on a burst from an interesting hard X-ray transient, the system on-board can rapidly re-point the satellite in order to bring the source in the narrower field of view of the other two telescopes on-board, the X-Ray Telescope (XRT; Burrows et al. 2005) and the Ultraviolet/Optical Telescope (UVOT; Roming et al. 2005). In this section we present the results obtained from our analysis of the *Swift* BAT and XRT observations of AXP 1E 1547.0–5408 performed during its bursting activity on 2008 October, being the source too absorbed to be detected with the UVOT.

2.1 Burst Alert Telescope data

On 2008 October 3 at 09:28:08 UT BAT triggered on and localized a short burst from a position consistent with that of the AXP 1E 1547.0–5408 (trigger 330353; Krimm et al. 2008a) which was followed by several other bursts extending to at least 09:38:24 UT. About 2 hours later, at 11:16:13 UT, BAT detected one last, bright burst which reached a peak count rate of $\sim 20\,000$ counts s⁻¹ in the 15–350 keV band (trigger 330367; Krimm et al. 2008b). The BAT time coverage of the source was discontinuous along the bursting period, totalling an effective exposure time of 4 ks (see Figure 1).

Datasets containing information for individual photons (event data) and data composed of 80-channel histograms with a typical integration time of ~ 5 minutes (survey data) were distributed. In the following, we present the results of our analysis for the bursts detected in the event data.

The data reduction was performed using version 2.9 of the standard *Swift*/BAT software distributed within FTOOLS under the HEASOFT package (version 6.5.1). A weight map, taking into account the contribution from the source to the counts in each BAT

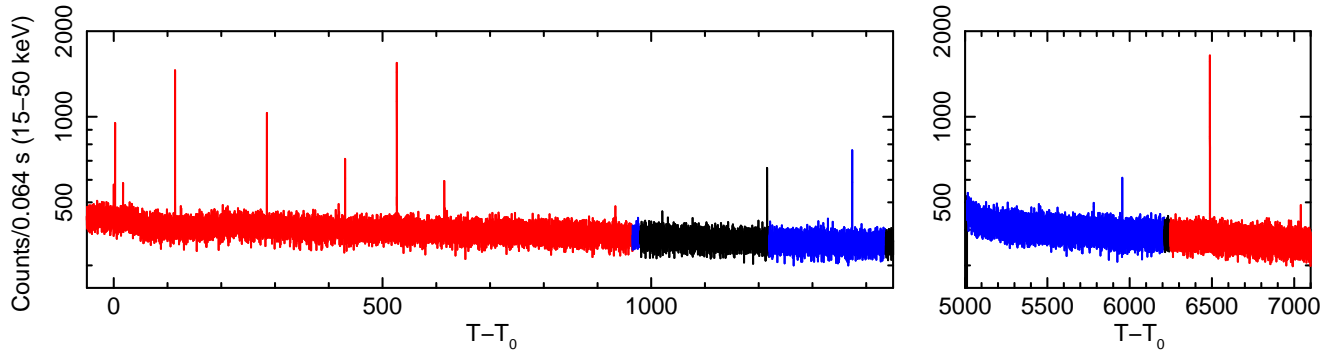


Figure 1. The light curve of 1E 1547.0–5408 generated on-board by the *Swift* Burst Alert Telescope (rate data). Black correspond to temporal ranges for which only rate data were available, red and blue to the temporal ranges for which also event and survey data, respectively, were distributed. T_0 corresponds to the first BAT trigger (trigger 330353; 2008-10-03 09:28:08 UT). The units of the horizontal axis variable are seconds.

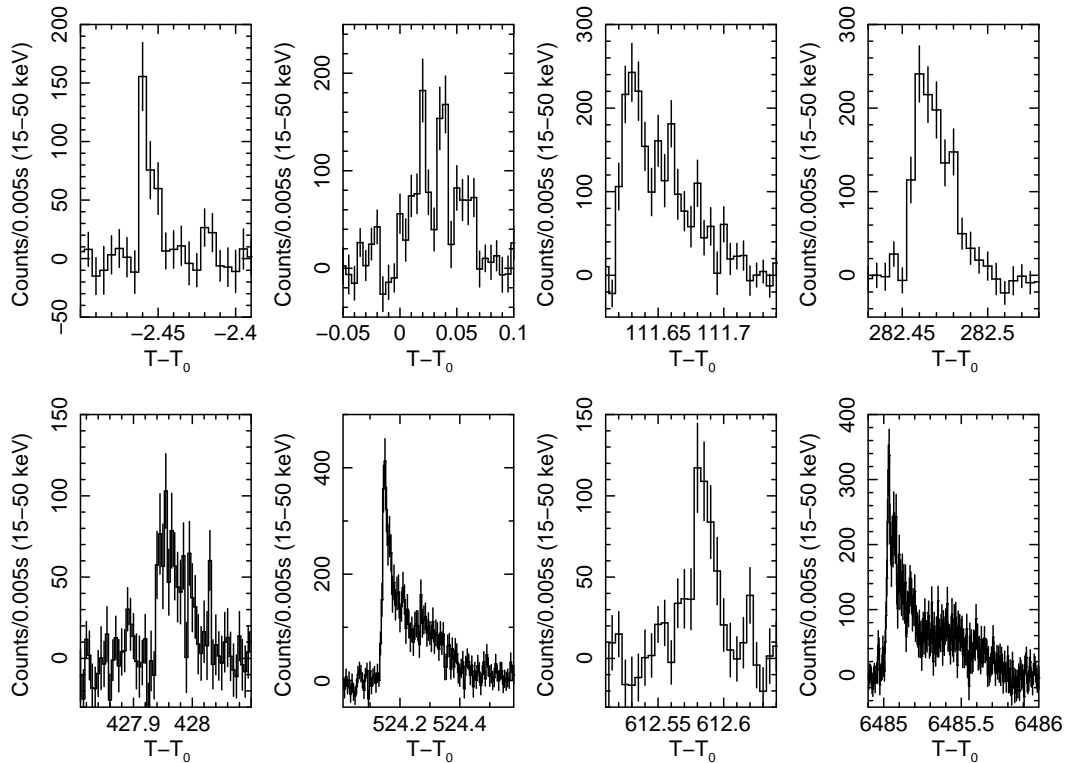


Figure 2. *Swift*/BAT background subtracted light curves of the 1E 1547.0–5408 bursts. Time bins are of 5 ms. The units of the horizontal axis variable are seconds. Negative times marks the not triggered burst few seconds before T_0 .

detector (mask-weighting technique),¹ was applied in order to obtain the background-subtracted counts of the source.

In Figure 2 the 15–50 keV light curves of bursts with more than 350 counts are plotted. For each burst we extracted a spectrum. All spectra are fitted well by a single blackbody model (BB) with a temperature of about 11 keV and an emitting radius of about 1 km (see Table 1). The limited statistics of BAT spectra did not allow us to check whether an additional BB component is present similar to the case of SGR 1900+14 (Israel et al. 2008b). We also tried to fit the 15–100 keV spectra with a power law and an optically thin thermal bremsstrahlung obtaining worse reduced χ^2 val-

ues (in the $1.4 \div 1.6$ and $1.7 \div 2.9$ range for the faintest and brightest bursts, respectively, and for 38 degree of freedom). The characteristic time-scales τ of each burst decay was also inferred by fitting the corresponding light curves with one or two (for the longest events) exponential laws and are reported in Table 1.

Whenever the bursts had sufficient statistics, time-resolved spectra were generated corresponding to the rise, peak, and decay phases of the bursts. The results of the fitting procedure is reported in Table 1. No significant variations were found in the spectral parameters, except for the normalization factor due to the luminosity evolution (decay) during the burst. On the other hand, time-resolved spectra show a moderate spectral evolution with the peak BB temperature being systematically softer than that during decay (similar results were obtained for SGR 1806–20 and

¹ See

<http://heasarc.nasa.gov/docs/swift/analysis/threads/batfluxunitsthread.html>.

Table 1. Spectral fit results (in the 15–100 keV range) of the bright bursts detected by *Swift*/BAT for the BB model. We assume a distance to the source of 4 kpc. T_0 corresponds to the first BAT trigger (2008-10-03 09:28:08) and errors are reported at 1σ confidence level.

Burst time (T- T_0)	τ (s)	Net counts	Duration (s)	kT (keV)	R (km)	L erg s $^{-1}$	Fluence erg cm $^{-2}$	χ_r^2 (d.o.f.)
-2.45	$0.007^{+0.002}_{-0.002}$	358	0.016	$10.1^{+0.9}_{-1.0}$	$1.5^{+0.3}_{-0.3}$	6.0×10^{38}	4.4×10^{-9}	0.93(38)
0	$0.018^{+0.005}_{-0.004}$	1492	0.070	$10.9^{+0.8}_{-0.8}$	$1.3^{+0.2}_{-0.2}$	6.4×10^{38}	2.1×10^{-8}	1.04(38)
111.6	$0.036^{+0.003}_{-0.003}$	2964	0.098	$12.4^{+0.6}_{-0.5}$	$1.2^{+0.1}_{-0.1}$	9.4×10^{38}	4.3×10^{-8}	1.18(38)
282.45	$0.015^{+0.001}_{-0.001}$	1451	0.035	$11.3^{+0.8}_{-0.7}$	$1.6^{+0.2}_{-0.2}$	1.1×10^{39}	1.9×10^{-8}	1.44(38)
427.9	$0.038^{+0.009}_{-0.007}$	988	0.100	$9.3^{+1.1}_{-1.0}$	$1.2^{+0.3}_{-0.2}$	2.8×10^{38}	1.3×10^{-8}	0.88(38)
524.2	$0.038^{+0.007}_{-0.005}$	8081	0.254	$11.8^{+0.3}_{-0.3}$	$1.4^{+0.1}_{-0.1}$	1.0×10^{39}	1.2×10^{-7}	0.80(38)
	$0.133^{+0.009}_{-0.008}$							
524.2 rise		310	0.010	$11.1^{+1.1}_{-1.0}$	$1.5^{+0.3}_{-0.3}$	8.6×10^{38}	4.0×10^{-9}	1.34(38)
524.2 peak		742	0.007	$8.3^{+0.4}_{-0.4}$	$4.6^{+0.5}_{-0.5}$	2.6×10^{39}	8.0×10^{-9}	1.01(38)
524.2 decay		7029	0.237	$11.9^{+0.3}_{-0.3}$	$1.3^{+0.1}_{-0.1}$	9.4×10^{38}	1.0×10^{-7}	0.94(38)
612.55	$0.012^{+0.003}_{-0.002}$	757	0.100	$11.1^{+1.3}_{-1.7}$	$0.7^{+0.3}_{-0.2}$	2.0×10^{38}	9.5×10^{-9}	0.92(38)
6485	$0.098^{+0.004}_{-0.004}$	14317	0.730	$10.8^{+0.3}_{-0.3}$	$1.3^{+0.1}_{-0.1}$	5.8×10^{38}	2.0×10^{-7}	1.17(38)
	$0.283^{+0.019}_{-0.018}$							
6485 rise		676	0.020	$9.6^{+1.0}_{-0.9}$	$2.0^{+0.4}_{-0.3}$	8.6×10^{38}	8.0×10^{-9}	0.82(38)
6485 peak		806	0.010	$7.4^{+0.3}_{-0.3}$	$5.0^{+0.5}_{-0.5}$	2.0×10^{39}	8.2×10^{-9}	1.03(38)
6485 decay		12835	0.700	$10.9^{+0.3}_{-0.3}$	$1.2^{+0.1}_{-0.1}$	5.6×10^{38}	1.8×10^{-7}	1.08(38)

SGR 1900+14: Götz et al. 2004, 2006; Israel et al. 2007b).

The presence of persistent emission during the non-bursting time intervals was also searched for in the event data. An image was generated from all the events of each file covering time intervals where no bursts were present and the standard source detection was run (BATCELLDETECT). Two time intervals were investigated, the first one ranging from $t = -41.5$ s to $t = 965.5$ s (net exposure time 1 001 s) and the second one from $t = 6 248.5$ s to $t = 7 300$ s (net exposure time 1 050 s). No significant emission in the direction of AXP 1E 1547.0–5408 were found. The 3σ upper limits on the flux in the 14–50 keV band for the two intervals described above are 6×10^{-10} and 2×10^{-10} erg cm $^{-2}$ s $^{-1}$, respectively.

2.2 X-Ray Telescope data

Swift executed a prompt slew on 1E 1547.0–5408 and the first XRT observation started only 99 s after the BAT trigger. Table 2 reports the log of the observations that were used for this work. The XRT uses a CCD detector sensitive to photons with energies between 0.2 and 10 keV. We considered Windowed Timing (WT) and Photon counting (PC) mode data. In PC mode the entire CCD is read every 2.507 s, while in WT mode only the central 200 columns are read and only one-dimensional imaging is preserved, achieving a time resolution of 1.766 ms (see Hill et al. 2004 for a detailed description of XRT modes).

The data were processed with standard procedures using the FTOOLS task XRTPipeline (version 0.12.0) and events with grades 0–12 and 0–2 were selected for the PC and WT data, respectively (see Burrows et al. 2005). For the timing and spectral analysis, we extracted the PC source events in the 0.5–10 keV range within a circle with a radius of 30 pixels ($\sim 71''$). The WT data (in the 0.5–10 keV range) were extracted in a rectangular region 40 pixels long (and 20 pixels wide) along the image strip. To estimate the background, we extracted PC events within an annular region (radii of 50 and 75 pixels) centered on the source and WT events within a

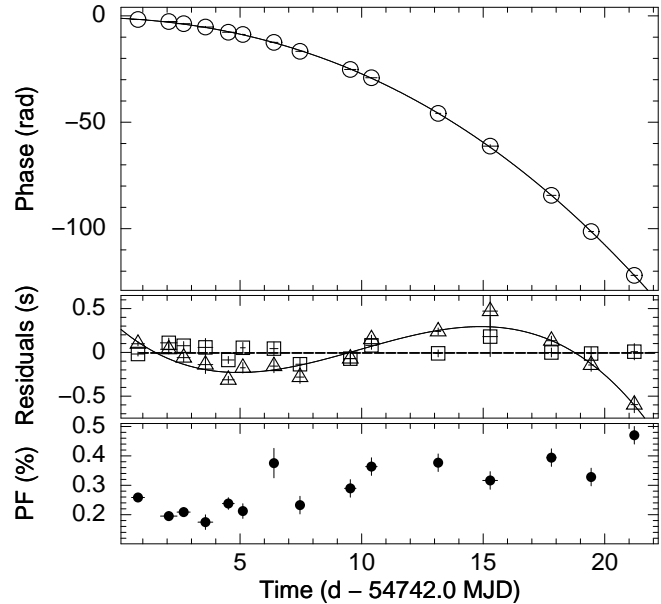


Figure 3. 0.5–10 keV *Swift*/XRT pulse phase evolution with time, together with the time residuals (central panel) with respect to the two phase-coherent timing solutions discussed in the text: $P-\dot{P}$ (triangles) and $P-\ddot{P}$ (squares). The solid lines in the upper panel represents the latter timing solution. The line in the central panel is the cubic fit to the $P-\dot{P}$ solution. The pulsed fraction (defined as the semi-amplitude of modulation divided by the mean source count rate) evolution is reported in the lower panel (where 0.2 means 20% pulsed fraction).

rectangular box (40×20 pixels) far from 1E 1547.0–5408.

Table 2. *Swift*/XRT observation log of 1E 1547.0–5408.

Sequence	Mode	Start time (UT) yyyy-mm-dd hh:mm:ss	End time (UT) yyyy-mm-dd hh:mm:ss	Exposure ^a (ks)	Time since trigger (d)
00330353000 ^b	PC	2008-10-03 09:29:47	2008-10-03 12:52:41	3.9	99 s
00330353001	WT	2008-10-03 12:54:35	2008-10-04 01:39:47	14.2	0.14
00330353002	WT	2008-10-04 17:27:08	2008-10-04 20:53:52	4.8	1.33
00330353004	WT	2008-10-05 09:42:43	2008-10-06 21:10:00	10.5	2.01
00330353005	WT	2008-10-07 06:39:12	2008-10-07 18:15:00	7.6	3.88
00330353006	WT	2008-10-08 00:20:12	2008-10-08 05:13:00	4.5	4.62
00330353007	WT	2008-10-09 05:20:33	2008-10-09 13:30:31	1.0	5.83
00330353008	WT	2008-10-10 07:05:50	2008-10-10 15:16:00	3.9	6.90
00330353010	WT	2008-10-12 07:11:17	2008-10-12 18:31:00	3.7	8.90
00330353011	WT	2008-10-13 04:05:15	2008-10-13 15:23:00	3.4	9.77
00330353012	WT	2008-10-16 01:05:20	2008-10-16 06:09:00	4.0	12.65
00330353013	WT	2008-10-17 23:38:20	2008-10-18 14:13:00	3.7	14.59
00330353014	WT	2008-10-20 14:47:50	2008-10-21 00:00:00	3.9	17.22
00330353015	WT	2008-10-22 08:03:14	2008-10-22 13:08:00	3.9	18.94
00330353016	WT	2008-10-24 01:56:29	2008-10-24 08:33:59	3.6	20.68

^a The exposure time is usually spread over several snapshots (single continuous pointings at the target) during each observation.

^b During this observation XRT repeatedly switched between PC and WT modes; since the exposure in WT is short (about 39 s), we did not include it in our analysis.

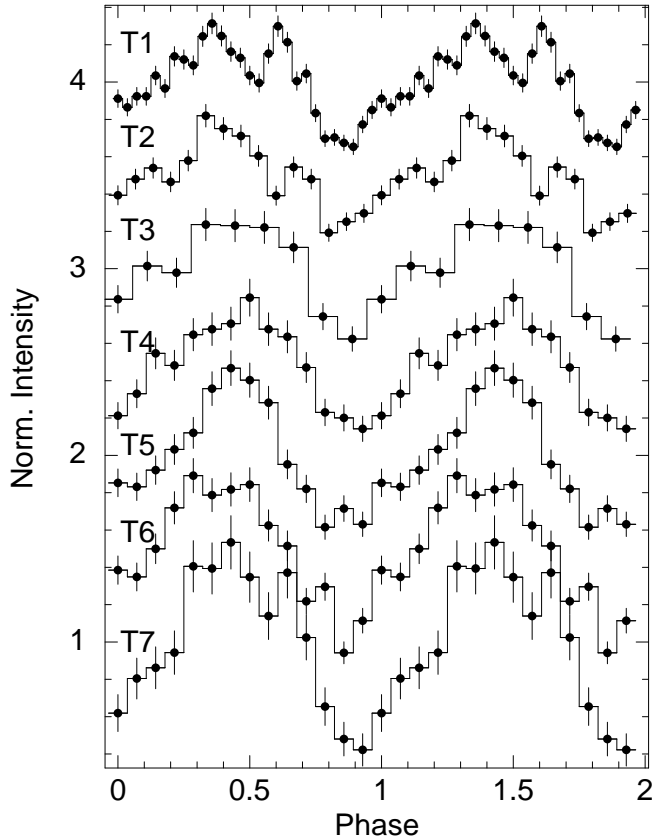


Figure 4. Time evolution of the 0.5–10 keV light curves folded by means of the $P-\dot{P}-\ddot{P}$ phase-coherent timing solution. Each light curve is covering approximately a three days time interval from the BAT trigger, where T1 to T7 correspond the the first and last time interval. Light curves are arbitrarily shifted along the vertical axis.

2.2.1 Timing

The 0.5–10 keV events were used to study the timing properties of the pulsar after having corrected the photon arrival times to the barycentre of the Solar system with the BARYCORR task (RA=15^h 50^m 54^s.12, Dec=−54° 18′ 24″.19 and J2000 was assumed for the source position; Israel et al. 2010). We started by inferring an accurate period measurement by folding the data from the first XRT pointing (in WT mode) at the period reported by Camilo et al. (2007b) and studying the phase evolution within the observation by means of a phase-fitting technique (details on this technique are given in Dall’Osso et al. 2003). Due to the high variability of the pulse shape we decided not to use a pulse template in the cross-correlation (which might artificially affect the phase shift), but to fit each individual folded light curve with the fundamental plus two higher harmonics. In the following we also implicitly assumed that the pulsation period (and its derivatives) is a reliable estimate of the spin period (and its derivatives), an assumption which is usually considered correct for isolated neutron stars. The resulting best-fit period ($\chi^2=1.1$ for 2 degree of freedom, hereafter d.o.f.) is $P = 2.071\,336(3)$ s (1σ c.l.; epoch 54742.0 MJD; see Esposito et al. 2008a). The above period accuracy of 3 μ s is enough to phase-connect coherently the later *Swift* pointings carried out on a daily baseline (see Table 2). Therefore, the procedure was repeated by adding, each time, a further *Swift* pointing. The relative phases were such that the signal phase evolution could be followed unambiguously for the whole *Swift* visibility window (see Figure 3). A quadratic term was clearly present in the phase time evolution since the very beginning. The resulting phase-coherent solution had a best-fit period $P = 2.071\,336\,8(3)$ s and period derivative $\dot{P} = 4.52(4) \times 10^{-11}$ s s^{−1} (MJD 54742.0 was used as reference epoch; 1σ c.l.). These values are in agreement (within $\sim 3\sigma$) with those, $P = 2.071\,335(1)$ s and $\dot{P} = 5.7(5) \times 10^{-11}$ s s^{−1}, reported by Israel et al. (2008a) and based on a reduced *Swift* dataset. The fit of the phases with a linear and a quadratic term remained statistically acceptable (reduced $\chi_r^2 \sim 0.8 \div 1.2$ for $8 \div 9$ d.o.f.) for the first two weeks since the BAT trigger. However, during the latest week the pulse phases increasingly deviate from

the extrapolation of the above $P-\dot{P}$ solution (see Figure 3 central panel, empty triangles), resulting in an unacceptable fit ($\chi_r^2 \sim 18$ for 12 d.o.f.). Therefore, we added a higher order component in order to take into account for the possible presence of a temporary or secular \ddot{P} term. The resulting new phase-coherent solution is $P = 2.0713401(7)$ s, $\dot{P} = 3.2(2) \times 10^{-11}$ s s $^{-1}$, and $\ddot{P} = 2.0(4) \times 10^{-17}$ s s $^{-2}$ (MJD 54742.0 was used as reference epoch; 1 σ c.l.; $\chi_r^2 = 2$ for 11 d.o.f.), or $\nu = 0.4827792(2)$ Hz, $\dot{\nu} = -7.4(5) \times 10^{-12}$ Hz s $^{-1}$, and $\ddot{\nu} = -4.8(9) \times 10^{-18}$ Hz s $^{-2}$. The time residuals with respect to the new timing solution are reported in Figure 3 (central panel; empty squares). The significance level for the inclusion of the cubic component is 5.1 σ . Moreover, the new timing solution implies a r.m.s. variability of only 0.08 s, corresponding to a timing noise level of about 3%, usually observed in isolated neutron stars. It is worth emphasizing that the second period derivative we found is very unlikely to be related to a random change of the pulse profiles which is expected to introduce only a random distribution of the phase residuals, rather than a cubic term. Recent studies on a sample of 366 radio pulsars showed that cubic terms on phase residuals are possible though smaller by several orders of magnitudes than that detected in 1E 1547.0–5408 and recorded on time-scales longer (years) than those we are sampling in our dataset (Hobbs 2010). More in general the (long-term) timing noise of young radio pulsars ($t < 10^5$ yr) can be explained as being caused by the recovery from previous glitch events (Hobbs 2010). The latter results make unlikely that the period second derivative is due to random noise. Finally, we note that in the above analysis we assumed that the emitting region is fixed in time with respect to the observer, as suggested by studies on other transient magnetars (see Perna & Gotthelf 2008; Albano et al. 2010). Correspondingly, we can also reasonably exclude that the cubic term is introduced by a random motion of the hot-spot.

Based on the above phase coherent solution we also studied the pulse shape and pulse fraction evolution. These are changing as shown in Figure 3 (lower panel) and Figure 4 as a function of time. In particular the pulsed fraction (semi-amplitude of the sinusoid divided by the mean count rate) has increased smoothly from 20% just after the outburst onset, up to almost 50% at the end of the *Swift* visibility window, 22 days after the BAT trigger. The pulse shape is variable too, from a multi-peak profile at the beginning of the outburst, to a less structured sinusoid during the latest XRT observations, though the lower statistics of the latter datasets might have hidden a more complex behavior. To assess the significance of the observed pulse shape variations as a function of time, we compared the folded pairs of contiguous lightcurves reported in Figure 4 by using a two-dimensional Kolmogorov-Smirnov test (Peacock 1983; Fasano & Franceschini 1987). The results show that the probability that they do not come from the same underlying distribution is $>9\sigma$ (T1-T2), $\sim 2.2\sigma$ (T2-T3), $\sim 3.3\sigma$ (T3-T4), $\sim 2.8\sigma$ (T4-T5), $\sim 3.8\sigma$ (T5-T6), and $\sim 2.9\sigma$ (T6-T7).

2.2.2 Spectroscopy

For the spectral fitting (with XSPEC version 12.4), the data were grouped so as to have at least 20 counts per energy bin. The ancillary response files were generated with XRTMKARF, and they account for different extraction regions, vignetting and point-spread function corrections. We used the latest available spectral redistribution matrix (v011) in CALDB.

Spectral modelling was performed by fitting together all the

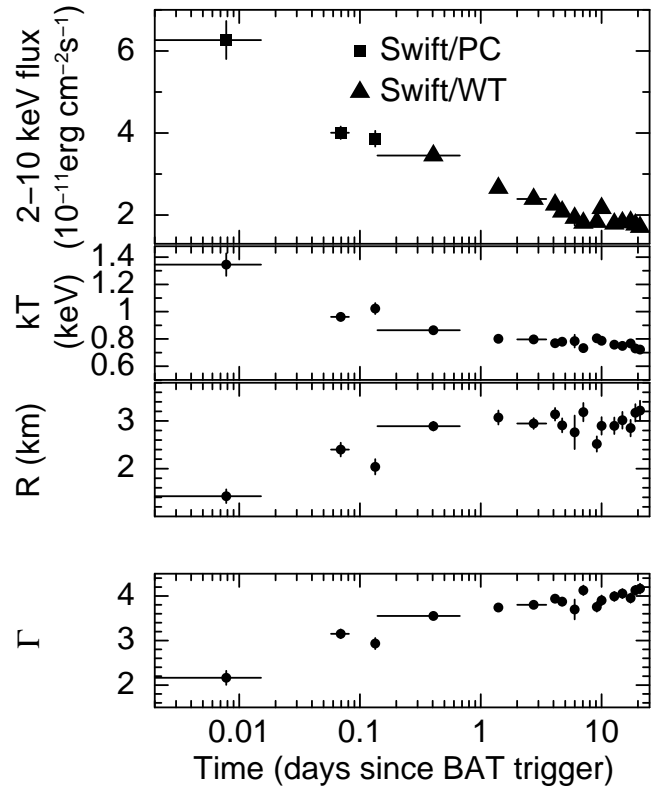


Figure 5. *Swift* XRT 2–10 keV observed fluxes (upper panel) as a function of the time since the BAT trigger. The two central panels show the evolution of the characteristic temperature (kT) and equivalent radius (R) of the blackbody model and inferred from the spectral fitting. The lowest panel shows the photon index (Γ) evolution by using a power-law component.

datasets in the 1–10 keV energy range (the high absorption value made the data below 1.5 keV almost useless). We first fit the spectra to simple models: a power law and a blackbody, both modified for interstellar absorption. All the parameters were left free to vary, except for the absorption column density, that was left free but with the request to be the same for all observations. Both models provide acceptable fits. The power-law fit ($\chi_r^2 = 1.04$ for 1292 d.o.f.) yields a column density $N_{\text{H}} = (6 \pm 1) \times 10^{22}$ cm $^{-2}$ and photon indices that increase from $\Gamma \simeq 2$ to 4 (see Figure 5, lower panel). In the data taken immediately after the first BAT trigger, 1E 1547.0–5408 was found to be in a record high state: the observed flux was $\sim 7 \times 10^{-11}$ erg cm $^{-2}$ s $^{-1}$ in the 2–10 keV band, about 100 times greater than that observed in 2008 July–September (Esposito et al. 2008a), and ~ 10 times greater than the previous highest recorded flux (Halpern et al. 2008). The observed flux declined by 70% in three weeks and the fading trend (see Figure 5, upper panel) can be described by a power-law with decay index $\alpha = -0.171 \pm 0.005$ (using the BAT trigger as origin of time).

From the blackbody fit ($\chi_r^2 = 1.02$ for 1292 d.o.f.) we derived a lower column density of $(2.50 \pm 0.06) \times 10^{22}$ cm $^{-2}$. Again there is a clear indication of spectral softening during the decay, with the blackbody temperature changing from $kT \simeq 1.3$ to 0.7 keV (while the radius increased from ~ 1 to 3 km).

For those observations for which the statistics was good enough (those obtained during the first day since the BAT trigger), the χ_r^2 was approximately in the 1.2–1.3 range (for 549 d.o.f.), suggesting a more complex spectrum. In order to check this issue, we re-analyzed the first four XRT/PC observations (see Table 2) fit-

ting a BB+PL model. The results are shown in Figure 6 and can be summarized as follows: (a) the first spectrum (99 s after the BAT trigger) can be totally ascribed to a hard power-law ($\Gamma = 1.1 \pm 0.2$, 90% c.l.), (b) during the second and the third observations (between 0.05 and 0.2 days after the trigger) the BB component becomes dominant ($kT = 0.75 \pm 0.05$ keV in both cases), though a PL component is still needed (but not statistically significant) above 4–6 keV, (c) after one day since the BAT trigger (fourth observation) the PL component is not any more detectable in the BB+PL model, while in the single PL model the photon index becomes >4 (mimicking a Wien tail of a BB component). Given the relatively low number of counts we did not attempt to fit more sophisticated and physical based models.

3 INTEGRAL OBSERVATION

Following the flux increase detected by *Swift*/XRT we triggered our *INTEGRAL* Target of Opportunity observation program. *INTEGRAL* (Winkler et al. 2003) observed the source from 2008 October 8 at 21:35 UT until October 10 at 04:53 UT for a total exposure time of 95.8 ks. We analyzed the IBIS (Ubertini et al. 2003) data, the coded mask imager on board *INTEGRAL*. In particular we selected the data derived from its low energy (15 keV–1 MeV) detector plane ISGRI (Lebrun et al. 2003), which is the most sensitive instrument below 100 keV.

We analyzed the 48 pointings that composed our observation, and derived the corresponding mosaicked images in two energy bands: 18–60 keV and 18–100 keV. The source is not detected during our observations, and the 3σ upper limits at the source position are 0.36 and 0.42 counts s^{-1} in the two energy bands respectively. This corresponds, assuming a power law spectral shape with photon index $\Gamma = 2.2$, to a flux upper limit of 1.8×10^{-11} erg cm^{-2} s^{-1} in the 18–60 keV band, and 2.5×10^{-11} erg cm^{-2} s^{-1} in the 18–100 keV band. Assuming a photon index $\Gamma = 1.5$ the upper limits are 2×10^{-11} erg cm^{-2} s^{-1} in the 18–60 keV band and 3×10^{-11} erg cm^{-2} s^{-1} in the 18–100 keV energy band.

In order to search for short bursts, we extracted event lists from each pointing. The events were then selected in energy (18–60 keV), and extracted from the pixels that were illuminated by the source direction for at least 60% of their surface. From these event lists, we derived light curves with a binning of 0.05 s. No burst was detected above the background level.

4 DISCUSSION AND CONCLUSIONS

Thanks to the *Swift* capability of detecting high energy impulsive events with the BAT, and of rapidly pointing to the BAT position with the narrow field instrument XRT, we had the chance of studying the short burst and long-term outbursting properties of one of the most interesting objects of the magnetar class, 1E 1547.0–5408, which entered a renewed phase of activity on 2008 October 3. In particular, given the relatively large period derivative of the source (Camilo et al. 2007b), we set up an observational strategy so that daily pointings were performed during a three week baseline (during which the source was observable by *Swift*). We studied the pulsed emission and inferred a rather accurate phase-connected timing solution which also includes a second derivative component. The spectral evolution was also studied as a function of the decreasing flux level.

The connection between the emission of short X-ray bursts and the increase of the persistent X-ray emission of AXPs and SGRs, has been reliably assessed in the last few years, especially thanks to the prompt *Swift* X-ray follow-up observations after the detection of short bursts in CXOU J164710.2–455216, SGR 1627–41, SGR 1900+14 and SGR 0501+4516 (Israel et al. 2007a; Esposito et al. 2008b; Israel et al. 2008b; Holland 2008; Rea et al. 2009). Furthermore, magnetar outbursts have been found to be characterized by an intensity-hardness correlation, the harder the more intense (and viceversa), as also observed in 1E 1547.0–5408. Both the connection with the occurrence of the bursts, and the hardness intensity correlation point toward a scenario in which these events are related to the evolution of a twisted magnetic field, which, once implanted by sudden crustal motions, necessarily decays (Thompson et al. 2002; Beloborodov 2008).

Particularly interesting are the burst energetics recorded by BAT. In fact, the 15–150 keV fluence of the bursts reported in Table 1 is in the $\sim 1 \times 10^{39}$ ergs range (inferred for a distance of 4kpc; Tiengo et al. 2010). These estimates are conservative lower limits to the total energy emitted in the bursts by the source. On the other hand, the upper limit on the persistent emission of the source, as seen by XRT, is of the order of $\sim 4 \times 10^{38}$ ergs (by integrating the exponential flux decay law from the beginning of October 2008 to mid-January 2009; see also first panel of Figure 5), corresponding to a ratio between energy released in the bursts and in the persistent tail >2 . The latter value is in between those observed for SGRs, i.e. >10 , and those of AXPs where the typical ratio is of the order of unity or less.

The X-ray timing properties of 1E 1547.0–5408 in October 2008 are such that a strong second derivative component, beside the usual P and \dot{P} ones, is needed in order to account for the evolution of the pulse phases during the about three weeks covered by *Swift* observations. The latter component is $\ddot{P} = 2.0(4) \times 10^{-17}$ s^{-2} or $\ddot{\nu} = -4.8(9) \times 10^{-18}$ $Hz s^{-2}$, therefore with the same sign as that of the first derivative. Second period derivatives have been detected only for a few AXPs/SGRs and, in all cases, occurred in response to glitches, such as in the case of 1RXS J1708–4009 (Dall’Osso et al. 2003; Israel et al. 2007b; Dib et al. 2008) and 1E 1841–045 (Dib et al. 2008), and/or outbursts, XTE J1810–197 (Camilo et al. 2007a) and SGR 0501+4516 (Israel et al. 2008c; Rea et al. 2009). In nearly all cases the second derivatives were relatively small, while the sign of these components was such that it acts in decelerating the spin down rates; typical $\ddot{\nu}$ values are approximately in the $0.05 \div 5 \times 10^{-21}$ $Hz s^{-2}$ range. Only for one AXP, namely 1RXS J1708–4009, negative second period derivatives in the $-0.01 \div -1.3 \times 10^{-20}$ $Hz s^{-2}$ range has been detected just after a glitch (Dib et al. 2008; Israel et al. 2007b).

The timing properties of 1E 1547.0–5408 were already known to be unusual during the first 6 months of radio monitoring (June – November 2007; Camilo et al. 2007b). Even in that case, observations were taken after a period of activity and also at that time both the first and second frequency derivatives were negative: $\dot{\nu} = -6.5 \times 10^{-13}$ $Hz s^{-1}$ and $\ddot{\nu} = -1.2 \times 10^{-19}$ $Hz s^{-2}$. Moreover, during the same time span in which the $\dot{\nu}$ (and torque) increased, the X-ray flux decreased, a property which is difficult to account for with simple assumptions. According to Camilo et al. (2007b), a possibility is that an extra torque (either than the magnetic spin down) originated from a particle wind that twists the magnetic field and, at the same time, transfers some angular momentum. In any case, the observed phenomenology calls for a mechanism in which X-ray luminosity and spin-down rate are not caused by the same mechanism or, at least, not by the same mech-

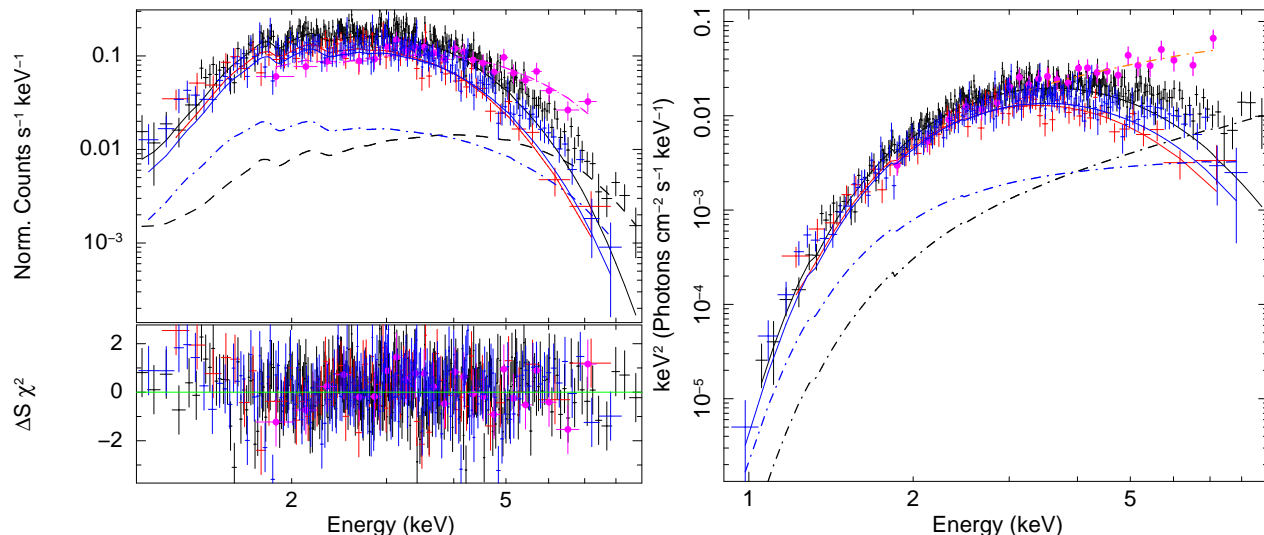


Figure 6. Left panel: *Swift* XRT spectra and residuals of the first four observations (listed in Table 2) carried out within ~ 1 day since the X-ray outburst of 1E 1547.0–5408 (pink filled circles, black, blue and red crosses, from the first to the fourth, respectively). The spectra are fitted by using a blackbody (solid lines) plus a power-law (dot-dash lines) model: the hard-to-soft evolution is evident (see text for details). Right panel: same as before but for the density flux in order to emphasize the spectral evolution above ~ 4 –5 keV.

anism and also at the same time. Even more dramatic is the case of October 2008 reported in this paper, with 1E 1547.0–5408 showing a $\dot{\nu}$ which is a factor of about 50 larger than in 2007, while the X-ray flux is a factor of 4–30 higher than during 2007. It is very likely that the $\dot{\nu}$ components related with glitch-only events have a different origin than those related to outburst events. For another transient AXP, XTE J1810–197, a $\dot{\nu}$ component has been detected during an outburst, although after two years since the onset (Camilo et al. 2007a). Correspondingly, a straightforward comparison with the 1E 1547.0–5408 properties is not feasible (similar arguments also hold for the radio properties of the two sources). In the case of SGR 0501+4516, the second derivative component was inferred during the first two months since the outburst onset and has a sign opposite to that of 1E 1547.0–5408.

A plausible scenario is that the dissimilar behavior seen in the various sources is related to the difference between the outburst \dot{P}_{outb} and the pulsar secular one \dot{P}_{sec} . Regardless of the mechanism responsible for the outburst and for the net timing effects at the outburst onset, it is reasonable to imagine the pulsar as a system which tends to recover its (almost) initial timing properties, i.e. same pre-outburst and post-outburst \dot{P}_{sec} (Alpar et al. 1984a,b; Link et al. 1992). Correspondingly, a negative or positive second period derivatives might be ascribed to whether the \dot{P}_{outb} over \dot{P}_{sec} ratio is larger or smaller than unity. Unfortunately, for all the four magnetars for which an outburst was detected in the latest few years (XTE J1810–197, CXOU J164710.2–455216, SGR 0501+4516 and 1E 1547.0–5408) the \dot{P}_{sec} is unknown. In the case of 1E 1547.0–5408 the positive second derivative detected in 2007 and 2008 would imply a \dot{P}_{outb} smaller than \dot{P}_{sec} : the latter being the value to which the source is approaching asymptotically. Within the classical scenario of isolated neutron stars, \dot{P}_{sec} is the spin-down value to be used when inferring the pulsar dipolar magnetic field strength. Correspondingly, the inferred value of $B_d \sim 2.7 \times 10^{14}$ Gauss should be considered as a lower limit on the intrinsic dipolar magnetic field strength.

Taken at face values, the increase of \dot{P} during the outburst decay appears difficult to reconcile with the predictions of the twisted magnetosphere model. In such model, in fact, the spin-down rate

is dictated by the radial variation of the external field. A globally twisted dipolar field has radial dependence $\sim R^{-2-p}$, where the index p decreases with increasing twist angle ($0 \leq p \leq 1$). If, as it seems natural to assume, the twist decays as the source returns to quiescence, one expects a decrease in the spin-down rate, i.e. a negative \dot{P} . As pointed out by Beloborodov (2008), however, in realistic situations the twist is likely to be confined to a rather narrow bundle of current-carrying field lines. In this case, and if the twist is suddenly implanted but its strength is moderate (twist angle less than ~ 1 rad), the twist may still grow for a while in spite of the luminosity released by dissipation monotonically decreasing. Only after the twist angle has reached its maximum value, it will start to decrease, together with the torque. This implies that the spin-down rate may be non-monotonic during the outburst decay, with a first phase characterized by a positive \dot{P} followed by a “recovery” during which $\dot{P} < 0$ and \dot{P} goes back to its secular value. The typical duration of the increasing spin-down stage is difficult to quantify, but it can last \sim months (see Eq. 55 in Beloborodov 2008). Indeed, this effect has been already proposed by Beloborodov (2008) to explain the anti-correlation between X-ray luminosity and torque observed in 1E 1048.1-5937 (Gavriil & Kaspi 2004). In 1E 1547.0–5408 \dot{P} has been observed to increase monotonically during summer/fall 2007 (during the decay of an outburst the peak of which has been missed; Camilo et al. 2008). The value of $\dot{\nu}$ corresponding to the latest radio observation of Camilo et al. (2008) is $\sim -7.35 \times 10^{-12} \text{ s}^{-2}$, and that in October 3, at the beginning of the X-ray outburst, $\sim -(7.4 \pm 0.4) \times 10^{-12} \text{ s}^{-2}$. A continuous decrease in $\dot{\nu}$ seems therefore hardly compatible with observations, and, since a constant $\dot{\nu}$ has never been observed in AXPs, it may well be that $\dot{\nu}$ started increasing at some epoch between 2007 November 22 (latest radio observations) and 2008 October 3 (X-ray outburst onset). This behavior would not be in contradiction with the untwisting magnetosphere model mentioned above. Finally, it is worth mentioning the possibility that the unusual \dot{P} behaviour after the October 2008 outburst might be one of the reasons for the extremely intense outburst displayed by 1E 1547.0–5408 in January 2009. In other words, the positive \dot{P} would be acted in accelerating the onset of stresses on the NS surface.

The pulsed fraction of 1E 1547.0–5408 clearly increases during October 2008, a behavior already observed during the initial phases of AXP outbursts, such as the case of CXOU J164710.2–455216 where the quiescent pulsed fraction ($\sim 80\%$) dropped to $\sim 10\%$ at the outburst onset and started increasing thereafter towards the quiescent value (Israel et al. 2007a; similar results have been recently obtained for SGR 0501+4516; Rea et al. 2009). However, in the case of 1E 1547.0–5408 the pulsed fraction at the outburst onset ($\sim 20\%$) is already larger than the quiescent value (as seen by *XMM-Newton*; $\sim 7\%$) and it reached $\sim 50\%$ at the end of the October 2008 *Swift* monitoring window. This finding, together with the very variable pulse profile as a function of time, suggests that the emission and/or magnetospheric geometry is complex and variable during the initial phases (on month timescales) of the outburst, and likely not easily related to the geometry in quiescence.

Pulsations in the X-ray flux may be a consequence of emission from a limited area of the star surface, of non-isotropic magnetospheric emission, or a combination of both effects. Again, if the star surface is heated by the returning currents which appear when a magnetospheric twist is implanted, even considering the simple evolution of the twist dictated by ohmic dissipation, an increase of the pulsed fraction in time is expected because, as time elapses, the bundle of current-carrying field lines shrinks and the heated area decreases. On the other hand, an increase in both pulsed fraction and emitting area, which is not excluded by the present data, would point toward a complete disassociation between the hot spot and the timing properties, with the latter perhaps of magnetospheric origin. The XRT statistics is not enough to unambiguously assess the evolution of the emitting area, nor even the presence of two distinct spectral components (BB and PL) detected by *XMM-Newton* in 2006 and 2007, although there are several hints suggesting that also in the spectra observed during October 2008 two components are needed.

Overall, the spectral properties of 1E 1547.0–5408 are also very similar to those of other transient magnetars, with an evident decay of the flux and a softening of the emitted photons (at least in the 1–10 keV range) as the outburst evolves in time. The spectral softening is apparent while using both the BB and the PL spectral models. Referring, for concreteness, to the power-law model, the photon index switches from ~ 2 at the outburst onset to ~ 4 after ~ 10 d. A softening is expected if the spectrum originates in a globally twisted magnetosphere by resonant up-scattering. As the twist angle decreases the charge density decreases making scattering less efficient. This implies that the high-energy tail filled up by up-scattered thermal photons becomes less and less populated, producing a softening of the spectrum. This has been verified by detailed Monte Carlo simulations in the case of a globally twisted dipolar field (e.g. Nobili et al. 2008). Although no detailed model has been presented as yet, it seems likely that the same picture holds if a localized twist is considered instead. As it was mentioned earlier, the twist angle may still increase for a while following the onset of the outburst, which would be consistent with the negative \dot{P} , while its spatial extent decreases (Beloborodov 2008). This latter effect may compensate for the first one and be the main effect responsible for the spectral evolution: in particular, if the region in which photons can be efficiently scattered by the currents is reduced, a flux softening and decrease in luminosity are expected.

ACKNOWLEDGEMENTS

This research is based on observations with the NASA/UK/ASI *Swift* mission. We thank the *Swift* duty scientists and science planners for making these observations possible. The Italian authors acknowledge the partial support from ASI (ASI/INAF contracts I/088/06/0, I/011/07/0, AAE TH-058, AAE DA-044, and AAE DA-006). PE thanks the Osio Sotto city council for support with a G. Petrocchi fellowship. SZ acknowledges support from STFC. NR is supported by a Ramón y Cajal fellowship. DG acknowledges the CNES for financial support.

REFERENCES

- Albano A., Turolla R., Israel G. L., et al. 2010, *ApJ*, submitted
- Alpar M. A., Anderson P. W., Pines D., Shaham J., 1984, *ApJ*, 278, 791
- Alpar M. A., Pines D., Anderson P. W., Shaham J., 1984, *ApJ*, 276, 325
- Barthelmy S. D., Barbier L. M., Cummings J. R., Fenimore E. E., Gehrels N., Hullinger D., Krimm H. A., Markwardt C. B., Palmer D. M., Parsons A., Sato G., Suzuki M., Takahashi T., Tashiro M., Tueller J., 2005, *Space Science Reviews*, 120, 143
- Beloborodov A. M., 2009, *ApJ*, 703, 1044
- Bernardini F., Israel G. L., Dall’Osso S., Stella L., Rea N., Zane S., Turolla R., Perna R., Falanga M., Campana S., Götz D., Mereghetti S., Tiengo A., 2009, *A&A*, 498, 195
- Burgay M., Rea N., Israel G. L., Possenti A., Burderi L., di Salvo T., D’Amico N., Stella L., 2006, *MNRAS*, 372, 410
- Burrows D. N., Hill J. E., Nousek J. A., Kennea J. A., Wells A., Osborne J. P., Abbey A. F., Beardmore A., et al. 2005, *Space Science Reviews*, 120, 165
- Camilo F., Ransom S. M., Halpern J. P., Reynolds J., Helfand D. J., Zimmerman N., Sarkissian J., 2006, *Nature*, 442, 892
- Camilo F., Cognard I., Ransom S. M., Halpern J. P., Reynolds J., Zimmerman N., Gotthelf E. V., Helfand D. J., Demorest P., Theureau G., Backer D. C., 2007a, *ApJ*, 663, 497
- Camilo F., Ransom S. M., Halpern J. P., Reynolds J., 2007b, *ApJ*, 666, L93
- Camilo F., Reynolds J., Johnston S., Halpern J. P., Ransom S. M., 2008, *ApJ*, 679, 681
- Dall’Osso S., Israel G. L., Stella L., Possenti A., Perozzi E., 2003, *ApJ*, 599, 485
- Dib R., Kaspi V. M., Gavriil F. P., 2008, *ApJ*, 673, 1044
- Duncan R. C., Thompson C., 1992, *ApJ*, 392, L9
- Esposito P., Israel G. L., Rea N., Krimm H. A., Palmer D. M., Gehrels N., Barthelmy S. D., Mereghetti S., Tiengo A., Gotz D., 2008a, *Astron. Tel.*, 1763
- Esposito P., Israel G. L., Zane S., Senziani F., Starling R. L. C., Rea N., et al. 2008b, *MNRAS*, 390, L34
- Fasano G., Franceschini A., 1987, *MNRAS*, 225, 155
- Gavriil F. P., Kaspi V. M., 2004, *ApJ*, 609, L67
- Gehrels N., Chincarini G., Giommi P., Mason K. O., Nousek J. A., Wells A. A., White N. E., Barthelmy S. D., et al. 2004, *ApJ*, 611, 1005
- Gelfand J. D., Gaensler B. M., 2007, *ApJ*, 667, 1111
- Gotthelf E. V., Halpern J. P., Buxton M., Bailyn C., 2004, *ApJ*, 605, 368
- Gotthelf E. V., Halpern J. P., 2005, *ApJ*, 632, 1075
- Götz D., Mereghetti S., Mirabel I. F., Hurlley K., 2004, *A&A*, 417, L45

- Götz D., et al., 2006, *A&A*, 445, 313
- Halpern J. P., Gotthelf E. V., Reynolds J., Ransom S. M., Camilo F., 2008, *ApJ*, 676, 1178
- Helfand D. J., Chatterjee S., Briskin W. F., Camilo F., Reynolds J., van Kerkwijk M. H., Halpern J. P., Ransom S. M., 2007, *ApJ*, 662, 1198
- Hill J. E., Burrows D. N., Nousek J. A., Abbey A. F., Ambrosi R. M., Bräuninger H. W., Burkert W., Campana S., et al. 2004, in Flanagan K. A., Siegmund O. H. W., eds, X-ray and Gamma-ray instrumentation for Astronomy XIII. Vol. 5165 of SPIE Conference Series, Bellingham WA, Readout modes and automated operation of the Swift X-ray Telescope. pp 217–231
- Hobbs G., Lyne A. G., Kramer M., 2010, *MNRAS*, 402, 1027
- Holland S. T. et. al., 2008, *GCN Circ.*, 8112
- Ibrahim A. I., Markwardt C. B., Swank J. H., Ransom S., Roberts M., Kaspi V., Woods P. M., Safi-Harb S., Balman S., Parke W. C., Kouveliotou C., Hurley K., Cline T., 2004, *ApJ*, 609, L21
- Israel G., Stella L., Covino S., Campana S., Angelini L., Mignani R., Mereghetti S., Marconi G., Perna R., 2004, in IAU Symposium Unveiling the Multi-wavelength Phenomenology of Anomalous X-ray Pulsars. p. 247
- Israel G. L., Campana S., Dall’Osso S., Muno M. P., Cummings J., Perna R., Stella L., 2007a, *ApJ*, 664, 448
- Israel G. L., Götz D., Zane S., Dall’Osso S., Rea N., Stella L., 2007b, *A&A*, 476, L9
- Israel G. L., Esposito P., Rea N., Krimm H. A., Palmer D. M., Gehrels N., Mereghetti S., Tiengo A., Senziani F., Gotz D., Zane S., 2008a, *Astron. Tel.*, 1770
- Israel G. L., Romano P., Mangano V., Dall’Osso S., Chincarini G., Stella L., Campana S., Belloni T., Tagliaferri e. a., 2008b, *ApJ*, 685, 1114
- Israel G. L., Woods P., Dall’Osso S., Esposito P., Rea N., Kouveliotou C., Mangano E. G. V., Romano P., Palmer D., Gehrels N., Stella L., Zane S., 2008c, *Astron. Tel.*, 1837
- Israel G. L., Rea N., Rol E., Mignani R., Testa V., Stella L., Esposito P., Mereghetti S., Tiengo A., Marconi G., Burgay M., Possenti A., Zane S., 2009, *Astron. Tel.*, 1909
- Israel G. L., et al., 2010, in preparation
- Krimm H. A., Beardmore A. P., Burrows D. N., Capalbi M., Evans P. A., Gehrels e. a., 2008a, *GCN Circ.*, 8311
- Krimm H. A., Beardmore A. P., Gehrels N., Page K. L., Palmer D. M., Starling R. L. C., Ukwatta T. N., 2008b, *GCN Circ.*, 8312
- Lebrun F., Leray J. P., Lavocat P., Crétolle J., Arquès M., Blondel C., Bonnin C., Bouère A., Cara C., Chaleil T. e. a., 2003, *A&A*, 411, L141
- Link B., Epstein R. I., Baym G., 1992, *ApJ*, 390, L21
- Mereghetti S., 2008, *A&A Rev.*, 15, 225
- Mignani R. P., Rea N., Testa V., Israel G. L., Marconi G., Mereghetti S., Jonker P., Turolla R., Perna R., Zane S., Lo Curto G., Chaty S., 2009, *A&A*, 497, 451
- Muno M. P., Gaensler B. M., Clark J. S., de Grijs R., Pooley D., Stevens I. R., Portegies Zwart S. F., 2007, *MNRAS*, 378, L44
- Nobili L., Turolla R., Zane S., 2008, *MNRAS*, 386, 1527
- Peacock J. A., 1983, *MNRAS*, 202, 615
- Perna R., Gotthelf E. V., 2008, *ApJ*, 681, 522
- Rea N., Zane S., Turolla R., Lyutikov M., Götz D. 2008, *ApJ*, 686, 1245
- Rea N., Israel G. L., Turolla R., Esposito P., Mereghetti S., Götz D., Zane S., Tiengo A., et al. 2009, *MNRAS*, 396, 2419
- Roming P. W. A., Kennedy T. E., Mason K. O., Nousek J. A., Ahr L., Bingham R. E., Broos P. S., Carter M. J., et al. 2005, *Space Science Reviews*, 120, 95
- Thompson C., Duncan R. C., 1993, *ApJ*, 408, 194
- Thompson C., Lyutikov M., Kulkarni S. R., 2002, *ApJ*, 574, 332
- Tiengo A., et al., 2010, *ApJ*, 710, 227
- Ubertini P., Lebrun F., Di Cocco G., Bazzano A., Bird A. J., Broenstad K., Goldwurm A., La Rosa G., et al. 2003, *A&A*, 411, L131
- Winkler C., Courvoisier T. J.-L., Di Cocco G., Gehrels N., Giménez A., Grebenev S., Hermsen W., Mas-Hesse J. M., et al. 2003, *A&A*, 411, L1
- Zane S., Rea N., Turolla R., Nobili L., Götz 2009, *MNRAS*, 398, 1403

This paper has been typeset from a $\text{\TeX}/\text{\LaTeX}$ file prepared by the author.